IEEE Access
Multidisciplinary ⋮ Rapid Review ⋮ Open Access Journal

Received 6 November 2024, accepted 26 November 2024, date of publication 2 December 2024,
date of current version 10 December 2024.

Digital Object Identifier 10.1109/ACCESS.2024.3509856

RESEARCH ARTICLE

Performance Analysis of Ergodic Rate and Effective Capacity for RIS-Assisted NOMA Networks Over Nakagami-*m* Fading Environments

TRAN CONG HUNG[1], TAN N. NGUYEN[2,3], (Member, IEEE), VU QUANG SY[4], ANH-TU LE[3], (Member, IEEE), BUI VU MINH[5], AND MIROSLAV VOZNAK[3], (Senior Member, IEEE)

[1]School of Computer Science and Engineering, The Saigon International University, Ho Chi Minh City 70000, Vietnam
[2]Communication and Signal Processing Research Group, Faculty of Electrical and Electronics Engineering, Ton Duc Thang University, Ho Chi Minh City 70000, Vietnam
[3]Faculty of Electrical Engineering and Computer Science, VSB–Technical University of Ostrava, 708 00 Ostrava, Czechia
[4]Faculty of Electrical and Electronics Engineering, Ton Duc Thang University, Ho Chi Minh City 70000, Vietnam
[5]Faculty of Engineering and Technology, Nguyen Tat Thanh University, Ho Chi Minh City 754000, Vietnam

Corresponding author: Vu Quang Sy (vuquangsy@tdtu.edu.vn)

This work was supported in part by the European Union within the REFRESH Project-Research Excellence For Region Sustainability and High-Tech Industries of the European Just Transition Fund under Grant CZ.10.03.01/00/22_003/0000048; and in part by the Ministry of Education, Youth, and Sports of the Czech Republic (MEYS CZ) through the Project SGS conducted by VSB–Technical University of Ostrava under Grant SP 061/2024.

ABSTRACT Massive connectivity and green communication will be important problems for the upcoming sixth generation (6G). Reconfigurable intelligent surfaces (RIS) and non-orthogonal multiple access (NOMA) have recently been presented as two major solutions to address the aforementioned issues. The main purpose of this paper is to investigate a downlink RIS-aided NOMA system in which the source intends to communicate with the two NOMA consumers over RIS for solving above problems. Our contributions include studying system performance in terms of ergodic rate and effective capacity, which is an essential assessment measure for delay-sensitive systems. In particular, we obtain analytical formulas for the ergodic rate and the effective capacity of nearby and distant users. In addition, we present orthogonal multiple access (OMA) data for comparison. The followings are the findings of this paper: 1) the ergodic rate and effective capacity of RIS-NOMA networks are superior to those of RIS-assisted OMA networks; 2) the system performance of RIS-NOMA networks can be significantly improved as the number of reflecting elements and Nakafami-m factor increases to improve the ergodic rate and effective capacity of both two users; 3) when compared to OMA, NOMA system has higher ergodic rate and effective capacity due to the short transmission time.

INDEX TERMS Non-orthogonal multiple access, reconfigurable intelligent surface, ergodic capacity, effective capacity.

I. INTRODUCTION

Due to its high transmission rate, high reliability, high capacity, high spectrum efficiency, and high energy efficiency, sixth-generation (6G) has garnered a lot of interest in recent years [1]. Reconfigurable intelligent surface (RIS) is a brand-new kind of passive device made up of several two-dimensional artificial electromagnetic materials that is expected to be a strong candidate for the future 6G standard. As a result, it offers significant business and economic

The associate editor coordinating the review of this manuscript and approving it for publication was Mohammad J. Abdel-Rahman.

benefits to the sector and the Internet of Things (IoT) [2], [3], [4], [5]. The IoT application scenario combines a number of developing technologies, and it is now the subject of the most popular study. The development of the IoT has raised the bar for communication technologies. On the other hand, expensive hardware, widespread access, and high energy consumption are the key issues facing future wireless networks. Therefore, in order to satisfy the increasing demands of consumers for quality of service (QoS) and data rate, it is essential to identify solutions with low power consumption, low cost, high efficiency, and high economic advantages [6], [7]. Thankfully, passive technologies like ambient backscatter and RIS have been included in wireless communication research [8], [9], [10], [11], [12]. Research on RIS has so far covered a wide range of topics, including optimization of secrecy rate [13], investigation of outage performance [14], [15], [16], conjunction with unmanned aerial vehicle [17], etc. The reflected elements are regulated by phase angles, as opposed to backscatter. As a result, RIS outperforms in terms of reducing energy usage and hardware costs in wireless communication systems.

As a novel paradigm, RIS is furnished with several reflecting components made of two-dimensional electromagnetic artificial materials. The software regulates each reflecting component, allowing for flexible adjustment of the reflected radio frequency (RF) signal's phase and angle. The perfect result is achieved and the performance of wireless communication systems is enhanced by modifying the phase angle of RIS [18]. Buildings' outside surfaces, walls, and ceilings may all be outfitted with RIS in a variety of ways, effectively increasing channel capacity. It uses incredibly little electricity and is environmentally benign, both of which can help the communication systems' energy efficiency [19]. In comparison to earlier technologies, the RIS can govern wireless environment behavior in a predictable and programmable manner. Numerous studies have concentrated on these RIS components because of these benefits. For wireless communication networks powered by RIS, an outage-constrained beamforming method was put out in [20]. The capacity degradation issue of the RIS network with hardware deficiencies was examined by the authors of [21] and [22]. Additionally, several researchers examined RIS in conjunction with other promising technologies, including as non-orthogonal multiple access (NOMA) [23], [24], simultaneous wireless information and power transfer (SWIPT), and multiple input multiple output (MIMO) in the mmWave range. According to [25], a two-stage iterative reweighted technique was used to develop the channel estimate scheme of the RIS-aided MIMO system in order to get the ideal channel state information. According to [26], the authors suggested an adaptive phase shifter solution for a RIS-assisted MIMO system using mobile station feedback and hierarchical codebooks. A straightforward approach for RIS-assisted NOMA downlink transmission that can increase connectivity and spectrum efficiency was put out by Ding and Vincent Poor [27]. Additionally, the authors in [28] used the semidefinite relaxation approach to optimize the cumulative rate of all users. All of this research indicate that RIS has a promising future when used in conjunction with additional technologies.

Non-orthogonal multiple access (NOMA) NOMA is a prospective technology for B5G (beyond the fifth generation) that has gained a lot of interest in both academia and business. [29], [30], [31]. NOMA is seen as having clear advantages in addressing issues with device access and spectrum scarcity, and it works well to address QoS and large-scale access [32], [33], [34]. The essential tenet of NOMA is that numerous users share identical time/frequency domain capabilities at the transmitter and receiver and that the transmitter communicates the superposition codes of multiple users directly. Users are given power in an equitable manner, with channel gain being inversely correlated with power distribution. Accordingly, users with high channel gains allocated less power, and conversely. Through successive interference cancellation (SIC), the interference information may be obtained from the receivers [35]. In order to achieve this, NOMA technology has been widely acknowledged as a practical way to raise the caliber of mobile network access and as a potential future development. However, there are certain shortcomings with the NOMA technology. The application of NOMA technology necessitates complex equipment. With NOMA alone, it is challenging to obtain decent performance when the wireless system has a large user base. RIS, fortunately, offers a fresh thought for this circumstance. Numerous studies have also demonstrated how well RIS may boost the functionality of the NOMA system. In [36], NOMA and orthogonal multiple access (OMA) performance of the RIS-assisted downlink communication network were examined, and a low-complexity strategy with near-optimal performance was proposed. Reference [37] investigated the effects of coherent phase shifting and random discrete phase shifting on the NOMA system with RIS assistance. In [38] and [39], the effectiveness of physical layer security was investigated. The outage performance of RIS-aided NOMA system under hardware impairment was investigated in [40] and [41].

The current study on the RIS-aided NOMA network does not account for the influence of delay on system performance, which is primarily concerned with the analysis of channel capacity and outage likelihood, among other things. As a result, it is difficult to correctly understand the business requirements for real-time communication. You et al. introduced the idea of effective capacity in [42] with the intention of studying the impact of delay on the communication system. Effective capacity is employed to measure the availability of multiple wireless networks within the limits of latency QoS. Effective capacity is a key consideration when explaining the effects of statistical delay QoS on system performance. They all produced tractable formulations of effective capacity in both high and low

TABLE 1. Comparison between the novelty of our work and previous papers.

Ref./Prop.	RIS	Nakagami-m fading	NOMA	Ergodic Rate	Effective Capacity	Stochastic Geometry
[12]	✓	✓	X	X	X	X
[44]	✓	✓	✓	✓	X	X
[45]	✓	✓	✓	✓	X	✓
[46]	✓	✓	X	✓	X	X
[47]	✓	X	X	X	X	✓
Our study	✓	✓	✓	✓	✓	X

signal-to-noise ratio (SNR) regions in order to understand the influence of system characteristics and conduct future research.

The estimated effective rate of RIS-aided communications was explored using closed-form formulae in [43]. It does, however, analyze the standard Rayleigh channel case. In comparison to the preceding studies, the primary contribution of this research is to investigate the ergodic rates, the influence of delay on the RIS-assisted NOMA system performance, and to accommodate delay QoS requirements so that NOMA may be used for delay-sensitive transmissions. Table 1 shows the comparison between our work and related papers. The following are the specifics of this paper's contributions:

- We propose a RIS-aided NOMA network in which the source (S) provides data to two NOMA user and RIS with N reflection components. We integrate a fundamental performance assessment metric of ergodic rate and effective capacity into the investigated system to account for delay-sensitive needs.
- For our proposed RIS-NOMA network, we obtain the closed-form approximation rate for the ergodic rate of a pair of NOMA users across Nakagami-m fading channels. In terms of the ergodic rate, we show that RIS-NOMA outperforms RIS-OMA. We have evidence that the ergodic rate of RIS-NOMA increases as the number of reflecting components increases.
- We begin by calculating the approximate expressions for the distant user's effective capacity and the closed-form for the near user. The effective capacity of a RIS-aided NOMA system for the near user (D_1) and far user (D_2) are also derived.

The following are the primary notations used in this paper. We use capital boldface to signify a matrix and lowercase boldface to represent a vector in this work. For the expectation operation, we employ $\mathbb{E}[\cdot]$. $K_a(.)$ denotes Bessel functions of the second kind. The symbol $(.)^H$ represents the conjugate transpose of a matrix or vector. diag (.) represents a diagonal matrix. $\mathcal{CN} \sim (\mu, N_0)$ is the Gaussian with the mean μ and the variance N_0. The abbreviations and acronyms are presented in Section II.

II. SYSTEM MODEL AND CHANNEL CHARACTERISTICS

A. SYSTEM DESCRIPTION

In this paper, we consider the following RIS-aided NOMA network: a source (S), a RIS consisting of N reflection components, a far user (D_2) and a near user (D_1). Because

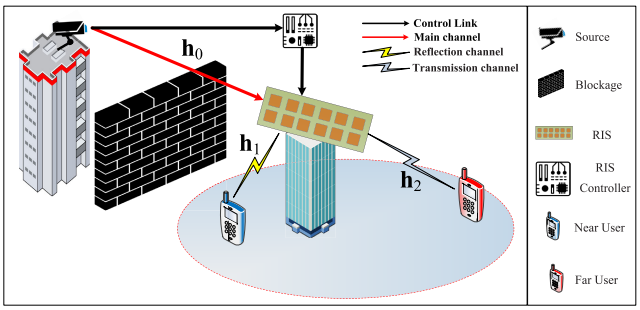

FIGURE 1. System model of NOMA-assisted RIS system.

of the obstructed and/or impediment, there is no direct link between the S and the users. We assume: (1) that all nodes have a single antenna; and (2) that all channels follow independent Nakagami-m fading. Let denote $\mathbf{h}_0 = \{h_{0,1}, \ldots, h_{0,n}, \ldots, h_{0,N}\}$ is the channel coefficients of S-RIS, $\mathbf{h}_1 = \{h_{1,1}, \ldots, h_{1,n}, \ldots, h_{1,N}\}$ is the channel coefficients of RIS-D_1, and $\mathbf{h}_2 = \{h_{2,1}, \ldots, h_{2,n}, \ldots, h_{2,N}\}$ is the channel coefficients of RIS-D_2. With the NOMA principle, the transmit power at S is P_S transmit the superposed signals $\sqrt{a_1 P_S}x_1 + \sqrt{a_2 P_S}x_2$, where x_1 and x_2 are the signals for D_1 and D_2, respectively, a_1, a_2 are the power allocation coefficients. The received signals at users are given as

$$\bar{y}_{D_1} = \underbrace{\mathbf{h}_1^H \Phi \mathbf{h}_0 \left(\sqrt{a_1 P_S}x_1 + \sqrt{a_2 P_S}x_2\right)}_{\text{Wanted signal}} + \underbrace{\omega_{D_1}}_{\text{AWGN}}, \quad (1)$$

$$\bar{y}_{D_2} = \underbrace{\mathbf{h}_2^H \Phi \mathbf{h}_0 \left(\sqrt{a_1 P_S}x_1 + \sqrt{a_2 P_S}x_2\right)}_{\text{Wanted signal}} + \underbrace{\omega_{D_2}}_{\text{AWGN}}, \quad (2)$$

where $\omega_{D_i} \sim \mathcal{CN}(0, N_0)$, $i \in \{1, 2\}$ is the additive white Gaussian noise (AWGN) with the power N_0. $\Phi \triangleq \text{diag}[\beta_1\phi_1, \beta_2\phi_2, \ldots, \beta_N\phi_N]$ is a diagonal matrix, which accounts for the effective phase shift applied by reconfigurable intelligent surfaces, $\beta_n \in [0, 1]$ represents the amplitude reflection coefficient of RIS, while $\phi_n = e^{j\theta_n}$, $j = \sqrt{-1}$, $\forall n = 1, 2, \ldots, N$ and $\theta_n \in [0, 2\pi)$ denotes the phase shift introduced by the n-th intelligent surface. It is assumed that the CSIs are perfectly known at the RIS controller [48], [49] and we set $\beta_1, \ldots, \beta_N = 1$ for simplicity.

For the RIS NOMA networks, the signal-plus-interference-to-noise ratio (SINR) at D_1 to decode the signal x_2 and x_1 by

using SIC are obtained as

$$\bar{\gamma}_{D_1,x_2} = \frac{a_2 P_S \left|\mathbf{h}_1^H \Phi \mathbf{h}_0\right|^2}{a_1 P_S \left|\mathbf{h}_1^H \Phi \mathbf{h}_0\right|^2 + N_0} = \frac{a_2 \rho \left|\mathbf{h}_1^H \Phi \mathbf{h}_0\right|^2}{a_1 \rho \left|\mathbf{h}_1^H \Phi \mathbf{h}_0\right|^2 + 1}, \tag{3}$$

$$\bar{\gamma}_{D_1,x_1} = a_1 \rho \left|\mathbf{h}_1^H \Phi \mathbf{h}_0\right|^2, \tag{4}$$

in which $\rho = \frac{P_S}{N_0}$ denotes the average transmit signal-to-noise radio (SNR). The SINR at D_2 to decode the own signal x_2 is given by

$$\bar{\gamma}_{D_2} = \frac{a_2 P_S \left|\mathbf{h}_2^H \Phi \mathbf{h}_0\right|^2}{a_1 P_S \left|\mathbf{h}_2^H \Phi \mathbf{h}_0\right|^2 + N_0} = \frac{a_2 \rho \left|\mathbf{h}_2^H \Phi \mathbf{h}_0\right|^2}{a_1 \rho \left|\mathbf{h}_2^H \Phi \mathbf{h}_0\right|^2 + 1}. \tag{5}$$

Let denote the phases of channels as $\bar{\theta}_n^1 = \bar{\theta}_n^0 + \bar{\theta}_n^1$ and $\bar{\theta}_n^2 = \bar{\theta}_n^0 + \bar{\theta}_n^2$. In this paper, we assume that $\theta_n^1 = -\bar{\theta}_n^1$ and $\theta_n^2 = -\bar{\theta}_n^2$, then we have $A = \sum_{n=1}^{N} \left|h_{0,n}\right| \left|h_{1,n}\right|$ and $B = \sum_{n=1}^{N} \left|h_{0,n}\right| \left|h_{2,n}\right|$. Next, Eqs. (4) and (5) are rewritten as

$$\bar{\gamma}_{D_1,x_1} = a_1 \rho |A|^2, \quad \bar{\gamma}_{D_2} = \frac{a_2 \rho |B|^2}{a_1 \rho |B|^2 + 1}. \tag{6}$$

B. CHANNEL CHARACTERISTICS

Then, under the Nakagami-m fading, the probability density function (PDF) and the cumulative distribution function (CDF) of $W = \{h_{0,n}, h_{1,n}, h_{2,n}\}$ respectively are given by [50]

$$f_{|W|}(x) = \frac{2x^{2m_W-1}}{\Gamma(m_W)} \left(\frac{m_W}{\Omega_W}\right)^{m_W} e^{-\frac{m_W x^2}{\Omega_W}}, \tag{7a}$$

$$F_{|W|}(x) = \frac{\gamma\left(m_W, \frac{m_W}{\Omega_W} x^2\right)}{\Gamma(m_W)}, \tag{7b}$$

where $\Gamma(\cdot)$ is the Gamma function, $\gamma(\cdot,\cdot)$ is the lower incomplete Gamma function, m_W is the shape parameter and $\Omega_W > 0$ denotes the average power of channel. The PDF of $Z_{Q_n^i}$, $i \in \{1,2\}$, $Q_n^i \triangleq \left|h_{0,n}\right| \left|h_{i,n}\right|$ can be calculated as

$$f_{Z_{Q_n^i}}(x) = \int_0^\infty \frac{1}{y} f_{h_{0,n}}(y) f_{h_{i,n}}\left(\frac{x}{y}\right) dy. \tag{8}$$

With help (7a) and [51, Eq. (3.471.9)], the PDF of $f_{Z_{Q_n^i}}(x)$ is given by

$$f_{Z_{Q_n^i}}(x) = \frac{4x^{m_{h_0}+m_{h_i}-1}}{\Gamma(m_{h_0})\Gamma(m_{h_i})} \left(\sqrt{\frac{m_{h_0} m_{h_i}}{\Omega_{h_0}\Omega_{h_i}}}\right)^{m_{h_0}+m_{h_i}} \times K_{m_{h_0}-m_{h_i}}\left(2\sqrt{\frac{m_{h_0} m_{h_i}}{\Omega_{h_0}\Omega_{h_i}}} x\right), \tag{9}$$

where $m_{h_0} = m_{h_{0,n}}$, and $m_{h_i} = m_{h_{i,n}}, \forall n$. Furthermore, the k-th moment of $Z_{Q_n^i}$, defined as $\mu_{Z_{Q_n^i}}(k) = \int_0^\infty x^k f_{Z_{Q_n^i}}(x) dx$. By using [51, Eq. (6.561.16)], the k-th moment $\mu_{Z_{Q_n^i}}(k)$ is obtained as follows

$$\mu_{Z_{Q_n^i}}(k) = \frac{\Gamma\left(m_{h_0} + k/2\right)\Gamma\left(m_{h_i} + k/2\right)}{\Gamma\left(m_{h_0}\right)\Gamma\left(m_{h_i}\right)} \left(\frac{\Omega_{h_0}\Omega_{h_i}}{m_{h_0} m_{h_i}}\right)^{\frac{k}{2}}. \tag{10}$$

With (7a) and (7b), it makes difficult to derive the expression closed-form of $Z_{Q_n^i}$. Thus, based on the k-th moment of Q_n^i, we can modify Q_n^i to Gamma distribution. Then, the PDF and CDF of Q_n^i is given as

$$f_{Q_n^i}(x) \approx \frac{\left(\beta_{Q_n^i}\right)^{\alpha_Q} x^{\alpha_{Q_n^i}-1}}{\Gamma\left(\alpha_{Q_n^i}\right)} e^{-\beta_{Q_n^i} x}, \tag{11a}$$

$$F_{Q_n^i}(x) \approx \frac{\gamma\left(\alpha_{Q_n^i}, \beta_{Q_n^i} x\right)}{\Gamma\left(\alpha_{Q_n^i}\right)}, \tag{11b}$$

in which

$$\alpha_{Q_n^i} = \frac{N\left(\mathbb{E}\left[Z_{Q_n^i}\right]\right)^2}{\mathrm{Var}\left[Z_{Q_n^i}\right]} = \frac{N\left[\mu_{Z_{Q_n^i}}(1)\right]^2}{\mu_{Z_{Q_n^i}}(2) - \left[\mu_{Z_{Q_n^i}}(1)\right]^2}, \tag{12a}$$

$$\beta_{Q_n^i} = \frac{\mathbb{E}\left[Z_{Q_n^i}\right]}{\mathrm{Var}\left[Z_{Q_n^i}\right]} = \frac{\mu_{Z_{Q_n^i}}(1)}{\mu_{Z_{Q_n^i}}(2) - \left[\mu_{Z_{Q_n^i}}(1)\right]^2}, \tag{12b}$$

where $\mathbb{E}[\cdot]$ and $\mathrm{Var}[\cdot]$ denote expectation operation and variance, respectively.

Define $X = Y^2$ with X and Y are arbitrary, we have $F_X(x) = F_Y\left(\sqrt{x}\right)$ and $f_X(x) = \frac{1}{2\sqrt{x}} f_Y\left(\sqrt{x}\right)$. Using this property, the PDF and CDF of $\left|Q_n^i\right|^2$ can be obtained as respectively

$$f_{|Q_n^i|^2}(x) = \frac{\left(\beta_{Q_n^i}\right)^{\alpha_{Q_n^i}} x^{\frac{\alpha_{Q_n^i}-2}{2}}}{2\Gamma\left(\alpha_{Q_n^i}\right)} e^{-\beta_{Q_n^i}\sqrt{x}}, \tag{13}$$

and

$$F_{|Q_n^i|^2}(x) = \frac{\gamma\left(\alpha_{Q_n^i}, \beta_{Q_n^i}\sqrt{x}\right)}{\Gamma\left(\alpha_{Q_n^i}\right)}. \tag{14}$$

III. ERGODIC RATE

In adaptive-rate transmission systems, the ergodic rate is a popular system performance statistic. The ergodic rates of two users for RIS-NOMA networks are examined in this section.

A. ERGODIC RATE OF D_1

According to the SIC principle, if D_1 correctly detects the signal of D_2, the attainable rate of D_1 may be given by $\mathcal{R}_{D_1} = \log\left(1 + \bar{\gamma}_{D_1,x_1}\right)$. Because of (6), the ergodic rate of D_1 for RIS-NOMA networks is stated as

$$\mathcal{R}_{D_1}^{erg} = \mathbb{E}\left\{\log_2\left(1 + \bar{\gamma}_{D_1,x_1}\right)\right\}. \tag{15}$$

The ergodic rate of D_1 is obtained in the following Proposition 1

Proposition 1: The closed-form approximation of Ergodic rate at user D_1 for RIS-NOMA can be given by

$$\mathcal{R}_{D_1}^{erg} \approx \frac{\pi^2 a_1 \rho}{4\Gamma\left(\alpha_{Q_n^1}\right) P \ln 2} \sum_{p=1}^{P} \sqrt{1-\upsilon_p^2} \times \sec^2\left(\frac{\pi\left(\upsilon_p+1\right)}{4}\right) \frac{\Gamma\left(\alpha_{Q_n^1}, \beta_{Q_n^1}\sqrt{\mathcal{G}\left(\upsilon_p\right)}\right)}{1+a_1\rho\mathcal{G}\left(\upsilon_p\right)}, \tag{16}$$

where $\mathcal{G}(t) = \tan\left(\frac{\pi(t+1)}{4}\right)$ and $\upsilon_p = \cos\left(\frac{2p-1}{2P}\pi\right)$.

Proof: See Appendix A.

B. ERGODIC RATE OF D_2

Assuming D_2 can detect its own signal x_2, $\mathcal{R}_{D_2} = \log\left(1+\bar{\gamma}_{D_2}\right)$ may be used to calculate D_2's feasible rate. The ergodic rate of D_2 is represented as

$$\mathcal{R}_{D_2}^{erg} = \mathbb{E}\left\{\log\left(1+\bar{\gamma}_{D_2}\right)\right\}. \tag{17}$$

Proposition 2: The closed-form approximation of ergodic rate at user D_2 for RIS-NOMA can be calculated as

$$\mathcal{R}_{D_2}^{erg} \approx \frac{\pi a_2}{2Pa_1\Gamma\left(\alpha_{Q_n^2}\right)\ln 2} \sum_{p=1}^{P} \frac{\sqrt{1-\upsilon_p^2}}{1+\Lambda\left(\upsilon_p\right)} \times \gamma\left(\alpha_{Q_n^2}, \beta_{Q_n^2}\sqrt{\frac{\Lambda\left(\upsilon_p\right)}{\rho\left(a_2-a_1\Lambda\left(\upsilon_p\right)\right)}}\right), \tag{18}$$

where $\Lambda(t) = \frac{a_2(t+1)}{2a_1}$ and υ_p has already been announced above.

Proof: See Appendix B.

IV. EFFECTIVE CAPACITY

The effective capacity is a combined mathematical framework described as the maximum constant arrival rate that the service process can maintain while meeting quality of service (QoS) standards [52]. In a block fading channel, the user's effective capacity is defined as

$$\mathcal{E}(\rho,\theta) = -\frac{1}{\zeta}\log_2\left(\mathbb{E}\left\{(1+\gamma)^{-\zeta}\right\}\right), \tag{19}$$

where $\zeta = \theta TB/\ln 2$ in which B is the block length and T is the bandwidth. $\theta > 0$ denotes a mathematical term that extends the idea of delay outage probability, and written by

$$\theta = -\lim_{x_{max}\to\infty} \frac{\ln\left[\Pr\left(Q > x_{max}\right)\right]}{x_{max}}, \tag{20}$$

where Q denote the steady-state queue length at the transmitter buffer and x_{max} is the predicted queue length threshold. $\theta \to \infty$ denotes a very severe delay requirement, whereas $\theta \to 0$ denotes a very lax delay need.

A. EFFECTIVE CAPACITY OF D_1

The definition's expression for the effective capacity of D_1 is calculated by

$$\mathcal{E}_{D_1} = -\frac{1}{\zeta}\log_2\left(\mathbb{E}\left\{\left(1+\bar{\gamma}_{D_1,x_1}\right)^{-\zeta}\right\}\right) = -\frac{1}{\zeta}\log_2\left(\int_0^\infty (1+x)^{-\zeta} f_{\bar{\gamma}_{D_1,x_1}}(x)\,dx\right). \tag{21}$$

Proposition 3: The analytical equation for the effective capacity of D_1 in the RIS NOMA networks is provided as

$$\mathcal{E}_{D_1} = -\frac{1}{\zeta}\log_2\left[\frac{\left(\beta_{Q_n^1}\right)^{\alpha_{Q_n^1}}\vartheta^{\frac{\alpha_{Q_n^1}-2}{2}}}{2\Gamma\left(\alpha_{Q_n^1}\right)} \sum_{k=0}^{K} \frac{(-1)^k\left(\beta_{Q_n^1}\sqrt{\vartheta}\right)^k}{k!\Gamma(\zeta)} \times\Gamma\left(\frac{\alpha_{Q_n^1}+k}{2}\right)\Gamma\left(\frac{2\zeta-\alpha_{Q_n^1}-k}{2}\right)\right], \tag{22}$$

where $\vartheta = \frac{1}{a_1\rho}$.

Proof: See Appendix C.

B. EFFECTIVE CAPACITY OF D_2

The definition states that the effective capacity of D_2 is represented as

$$\mathcal{E}_{D_2} = -\frac{1}{\zeta}\log_2\left(\mathbb{E}\left\{\left(1+\bar{\gamma}_{D_2}\right)^{-\zeta}\right\}\right) = -\frac{1}{\zeta}\log_2\left(\int_0^\infty (1+x)^{-\zeta} f_{\bar{\gamma}_{D_2}}(x)\,dx\right). \tag{23}$$

Proposition 4: The closed-form the effective capacity of D_2 in the RIS NOMA networks is provided by

$$\mathcal{E}_{D_2} \approx -\frac{1}{\zeta}\log_2\left[\frac{\pi a_2\left(\beta_{Q_n^2}\right)^{\alpha_{Q_n^2}}}{4Pa_1\Gamma\left(\alpha_{Q_n^2}\right)} \sum_{p=1}^{P} \frac{\sqrt{1-\upsilon_p^2}}{\left(1+\bar{\Lambda}\left(\upsilon_p\right)\right)^{\zeta}} \times\left(\frac{\bar{\Lambda}\left(\upsilon_p\right)}{\rho\left(a_2-a_1\bar{\Lambda}\left(\upsilon_p\right)\right)}\right)^{\frac{\alpha_{Q_n^2}-2}{2}} e^{-\beta_{Q_n^2}\sqrt{\frac{\bar{\Lambda}\left(\upsilon_p\right)}{\rho\left(a_2-a_1\bar{\Lambda}\left(\upsilon_p\right)\right)}}}\right], \tag{24}$$

Proof: See Appendix D.

V. NUMERICAL RESULTS

In this part, numerical findings for the performance evaluation of the considered network are provided. Meanwhile, the results of the Monte Carlo simulation are averaged across 10^6 separate runs. The fading parameters were set to $m = m_{h_0} = m_{h_1} = m_{h_2}$. We denote "Ana." and "Sim." as analytical computation and Monte-Carlo computing-based simulations, respectively, in the figures below. Table 2 shows the parameters. The Gauss-Chebyshev parameter is set to $P = 100$ in [53] for a close approximation simulation.

Figure 2 displays the ergodic rates of two users in RIS-NOMA networks compared to the transmit SNR. The

TABLE 2. The parameters for numerical results [54].

Parameter	Simulation Values
The power allocation factor of D_1	$a_1 = 0.1$
The power allocation factor of D_2	$a_2 = 0.9$
Number of RIS components (N)	$N = 16$
Fading Parameter	$m = 2$
Bandwidth	$B = 200$ kHz
Block length	$T = 6.5$ ms
QoS exponent	$\theta = 0.5$
Mean channel gains	$\Omega_{h_0} = \Omega_{h_1} = \Omega_{h_2} = 1$

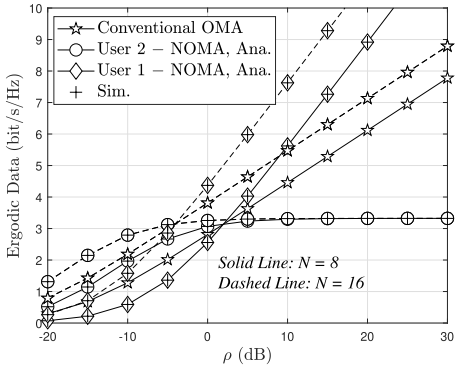

FIGURE 2. Ergodic rate versus transmit SNR at source.

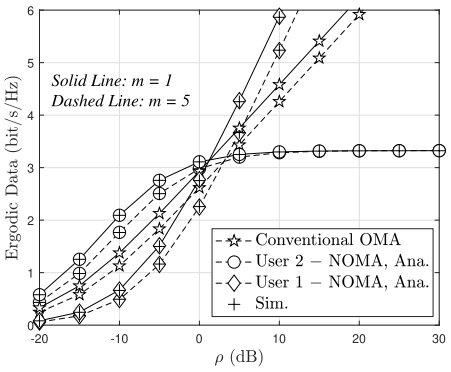

FIGURE 3. Impact of fading severity parameters on the ergodic rate, with $N = 8$.

picture shows that the ergodic rate curves Monte Carlo simulation and the generated analytical ergodic rate findings for RIS-NOMA are perfectly compatible, demonstrating the correctness of the derived theoretical ergodic rate results. The D_1 ergodic rate for RIS-NOMA is higher at high SNR than the user ergodic rate for RIS-OMA. The SNR slope of D_1 for RIS-NOMA is greater than that of D_1 for RIS-OMA, which explains this. D_2's ergodic rate for RIS-NOMA is lower at high SNR than D_1's for RIS-NOMA and user's for RIS-OMA. This is due to the fact that D_2 for RIS-NOMA has a smaller high SNR slope than both D_1 and the user for RIS-OMA.

Fig. 3 investigates the impacts of m on the ergodic rate performance. When $m = 5$, the ergodic rate performance

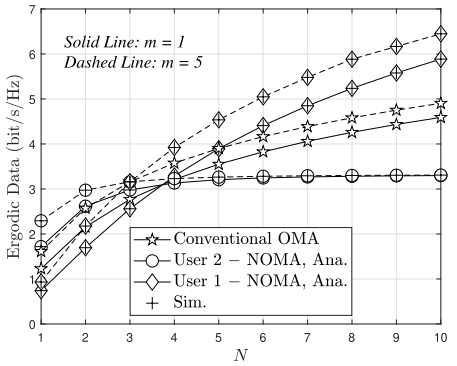

FIGURE 4. The ergodic rate versus N for various m, with $\rho = 10$ dB.

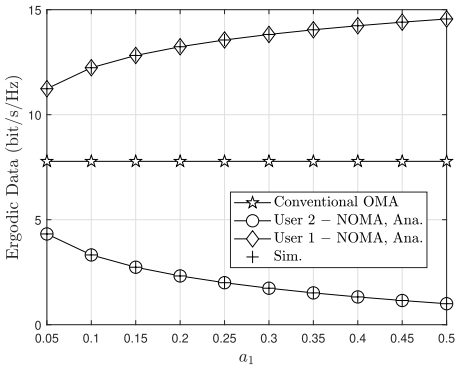

FIGURE 5. The impact of a_1 on ergodic rate, with $\rho = 30$ dB and $m = 2$.

for all ρ improves. Furthermore, performance improves as ρ increases. However, the curves saturate for D_2 when ρ is large, and when ρ is greater than 15 dB, performance improves at D_1 and Conventional OMA.

Fig. 4 depicts the effect of N on ergodic rate performance for different values of m when $\rho = 10$ dB. The ergodic rate performance increases with increasing N, but saturates for higher values of N at D_2, since the ergodic rate varies logarithmically with N, regardless of m.

According to Fig. 5, theoretical and simulation findings show that power allocation coefficient a_1 contributes considerably to performance indicators, such as ergodic rate. The rationale for the varied trends in ergodic capacity for two users is described by ρ, which relies heavily on such power coefficient; hence, the fairness of two users should be reasonably decided. Similarly, because there is no power allocation in the OMA situation, it is just influenced by ρ.

Fig. 6 shows the trends in the effective capacity of two users, the whole RIS-NOMA networks and conventional OMA in relation SNR. Next, we set N to 4, θ to 0.5, and m to 2. The correctness of the closed-form equations for the effective capacity in the instance of the RIS-NOMA networks is demonstrated in Fig. 6. The first point is that D_2's effective capacity performance is superior to D_1's. This benefit of D_2 is magnified in the case of high SNR regions. Furthermore, to compare the effective capacities of the RIS in OMA and NOMA situations, we give effective capacity

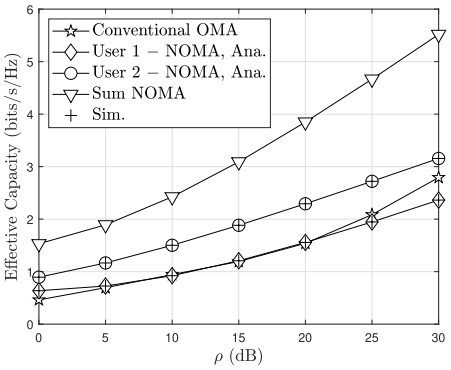

FIGURE 6. The effective capacity versus the transmit ρ in RIS-NOMA and RIS-OMA, with $N = 4$ and $m = 2$.

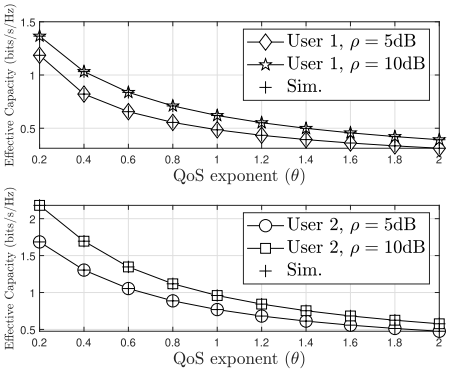

FIGURE 7. Effects of the QoS exponent θ on the effective capacity, with $m = 2$.

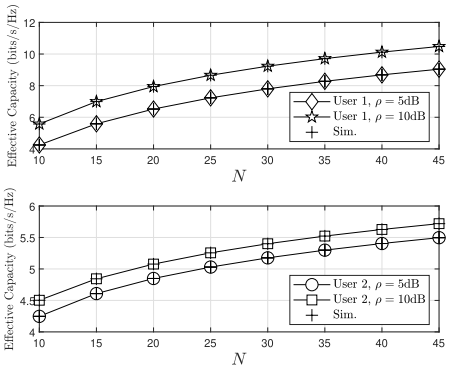

FIGURE 8. The number of RIS elements, with $m = 2$.

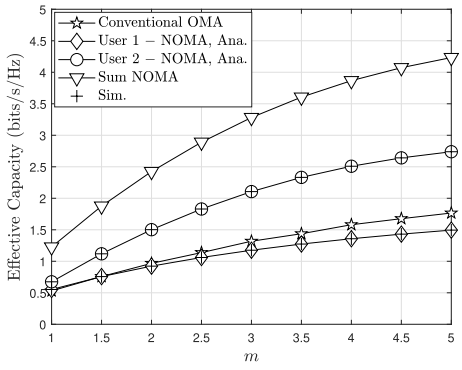

FIGURE 9. The effective capacity versus m in RIS-NOMA and RIS-OMA, with $N = 4$ and $\rho = 10$ dB.

curves for users and OMA. According to the simulation, the effective capacities of D_2 and D_1 rise monotonically with respect to SNR in the OMA situation. In addition, the total RIS-NOMA networks are shown in Fig. 6 with a triangular line. The effective capacity of RIS-NOMA networks as a whole is much greater than that of two users and traditional RIS-OMA networks. Finally, it is important to remember that, depending on the real situation, RIS-NOMA networks may adjust how much they reflect and/or transmit, which might lead to better performance.

Fig. 7 shows the influence of QoS exponent θ on effective capacity with $\rho = 5$dB and 10dB. As previously stated, a bigger θ indicates a tighter QoS delay requirement and a reduced effective capacity. When θ increases, the effective capacity of both D_1 and D_2 decreases to varying degrees. Concurrently, it is determined that a larger ρ indicates a greater effective capacity, which is also verified by Fig. 6. Increasing ρ, on the other hand, does not improve the effective capacity of D_1 as much as D_2.

We display Fig. 8 with the number of RIS elements as the variable to further explore and explain the relationship between the number of RIS elements and the effective capacity. We see that as the number of RIS elements rises, so does the effective capacity of D_1 and D_2. As anticipated, the addition of more RIS pieces would result in more spatial variety and improved user performance. The other finding is that a rise in ρ results in an increase in the effective capacity of users. In particular, it is shown that when the number of RIS elements is low, the value of ρ has a significant impact on the effective capacity of D_1.

Fig. 9 shows the influence of m on effective capacity with $N = 4$ and $\rho = 10$ dB. Sum NOMA consistently shows the highest effective capacity, indicating its superior performance compared to the other schemes. Conventional OMA has the lowest capacity, remaining relatively flat as m increases. The NOMA scheme for D_1 and D_2 shows improvements over OMA, with D_1 achieving slightly better performance than D_2. The simulation results closely match the analytical results, confirming the validity of the analysis. As m increases, the effective capacity for all schemes improves, with NOMA showing a significant advantage over OMA, particularly in the sum capacity.

VI. CONCLUSION

This study examines the system performance of RIS-assisted downlink NOMA communication networks in terms of effective capacity and ergodic rate over Nakagami-m fading channels. For RIS-NOMA networks, the precise and approximation formulae for the ergodic rate and effective capacity of two users have been found. The closed-form analytical formulations matched the Monte Carlo simulations quite

well. According to simulation studies, the ergodic rate and effective capacity of RIS-NOMA outperform that of RIS-OMA. Furthermore, it has been established that increasing the number of reflecting components and the Nakagami-m factor improves the system performance of RIS-NOMA networks. Finally, the theoretical direction provided by this analytical framework will be beneficial to the RIS-NOMA networks. We will explore expanding the research to include numerous users in the future based on this work. Furthermore, efficient power allocation and numerous antennas of device nodes are attractive research areas.

APPENDIX A
PROOF OF PROPOSITION 1

By replacing (6) in (15), the ergodic rate at D_1 can be calculated as

$$\mathcal{R}_{D_1}^{erg} = \mathbb{E}\left\{\log\left(1+a_1\rho|A|^2\right)\right\} = \frac{a_1\rho}{\ln 2}\int_0^{\infty}\frac{1-F_{|A|^2}(y)}{1+a_1\rho y}dy. \tag{25}$$

The CDF of $|A|^2$ can be written as

$$F_{|A|^2}(y) = \Pr\left(|A|^2 < x\right) = \frac{\gamma\left(\alpha_{Q_n^1}, \beta_{Q_n^1}\sqrt{x}\right)}{\Gamma\left(\alpha_{Q_n^1}\right)}. \tag{26}$$

Substituting (26) into (25), $\mathcal{R}_{D_1}^{erg}$ is written as

$$\mathcal{R}_{D_1}^{erg} = \frac{a_1\rho}{\Gamma\left(\alpha_{Q_n^1}\right)\ln 2}\int_0^{\infty}\frac{\Gamma\left(\alpha_{Q_n^1}, \beta_{Q_n^1}\sqrt{y}\right)}{1+a_1\rho y}dy. \tag{27}$$

Let $t = \frac{4}{\pi}\arctan(x) - 1 \Rightarrow \tan\left(\frac{\pi(t+1)}{4}\right) = x \Rightarrow \frac{\pi}{4}\sec^2\left(\frac{\pi(t+1)}{4}\right)dt = dx$ with $\sec(x) = \left(\frac{1}{\cos(x)}\right)$, (27) is expressed as

$$\mathcal{R}_{D_1}^{erg} = \frac{\pi a_1\rho}{4\ln 2}\int_{-1}^{1}\frac{\Gamma\left(\alpha_{Q_n^1}, \beta_{Q_n^1}\sqrt{\mathcal{G}(t)}\right)\sec^2\left(\frac{\pi(t+1)}{4}\right)}{\left(1+a_1\rho\mathcal{G}(t)\right)\Gamma\left(\alpha_{Q_n^1}\right)}dt, \tag{28}$$

where $\mathcal{G}(t) = \tan\left(\frac{\pi(t+1)}{4}\right)$.

Unfortunately, it is difficult to derive a closed-form expression for (28), an accurate approximation can be obtained using Gaussian-Chebyshev quadrature [55, Eq. (25.4.38)], $\mathcal{R}_{D_1}^{erg}$ is given as

$$\mathcal{R}_{D_1}^{erg} \approx \frac{\pi^2 a_1\rho}{4\Gamma\left(\alpha_{Q_n^1}\right)P\ln 2}\sum_{p=1}^{P}\sqrt{1-\upsilon_p^2} \times \sec^2\left(\frac{\pi(\upsilon_p+1)}{4}\right)\frac{\Gamma\left(\alpha_{Q_n^1}, \beta_{Q_n^1}\sqrt{\mathcal{G}(\upsilon_p)}\right)}{1+a_1\rho\mathcal{G}(\upsilon_p)}, \tag{29}$$

where $\upsilon_p = \cos\left(\frac{2p-1}{2P}\pi\right)$. This completes the proof.

APPENDIX B
PROOF OF PROPOSITION 2

Similar to the steps in Proof of proposition 1, $\mathcal{R}_{D_2}^{erg}$ can be calculated as

$$\mathcal{R}_{D_2}^{erg} = \mathbb{E}\left\{\log\left(1+\underbrace{\frac{a_2\rho|B|^2}{a_1\rho|B|^2+1}}_{Z}\right)\right\} = \frac{1}{\ln 2}\int_0^{\infty}\frac{1-F_Z(y)}{1+y}dy. \tag{30}$$

The CDF of Z can be written as

$$\mathcal{R}_{D_2}^{erg} = \frac{1}{\ln 2\,\Gamma\left(\alpha_{Q_n^2}\right)}\int_0^{\frac{a_2}{a_1}}\frac{\Gamma\left(\alpha_{Q_n^2}, \beta_{Q_n^2}\sqrt{\frac{y}{\rho(a_2-a_1y)}}\right)}{1+y}dy, \tag{31}$$

Note (31) is derived on the condition of $y < \frac{a_2}{a_1}$. Let $t = \frac{2a_1}{a_2}x - 1 \rightarrow \frac{a_2(t+1)}{2a_1} = x \rightarrow \frac{a_2}{2a_1}dt = dx$, the ergodic rate of D_2 is expressed as

$$\mathcal{R}_{D_2}^{erg} = \frac{a_2}{2a_1\Gamma\left(\alpha_{Q_n^2}\right)\ln 2}\int_{-1}^{1}\frac{1}{1+\Lambda(t)} \times \Gamma\left(\alpha_{Q_n^2}, \beta_{Q_n^2}\sqrt{\frac{\Lambda(t)}{\rho\left(a_2-a_1\Lambda(t)\right)}}\right)dt, \tag{32}$$

where $\Lambda(t) = \frac{a_2(t+1)}{2a_1}$.

Similarly with solving $\mathcal{R}_{D_1}^{erg}$, we using the Gaussian-Chebyshev quadrature, $\mathcal{R}_{D_2}^{erg}$ can be written as

$$\mathcal{R}_{D_2}^{erg} \approx \frac{\pi a_2}{2Pa_1\Gamma\left(\alpha_{Q_n^2}\right)\ln 2}\sum_{p=1}^{P}\frac{\sqrt{1-\upsilon_p^2}}{1+\Lambda(\upsilon_p)} \times \gamma\left(\alpha_{Q_n^2}, \beta_{Q_n^2}\sqrt{\frac{\Lambda(\upsilon_p)}{\rho\left(a_2-a_1\Lambda(\upsilon_p)\right)}}\right). \tag{33}$$

This completes the proof.

APPENDIX C
PROOF OF PROPOSITION 3

Based on the notion of effective capacity in (19), we can formulate the expression of effective capacity at D_1 as

$$\mathcal{E}_{D_1} = -\frac{1}{\zeta}\log_2\left(\int_0^{\infty}(1+x)^{-\zeta}f_{\bar{\gamma}_{D_1,x_1}}(x)\,dx\right) = -\frac{1}{\zeta}\log_2\left[\frac{\left(\beta_{Q_n^1}\right)^{\alpha_{Q_n^1}}\vartheta^{\frac{\alpha_{Q_n^1}-2}{2}}}{2\Gamma\left(\alpha_{Q_n^1}\right)} \times \int_0^{\infty}(1+x)^{-\zeta}x^{\frac{\alpha_{Q_n^1}-2}{2}}e^{-\beta_{Q_n^1}\sqrt{\vartheta x}}dx\right], \tag{34}$$

where $\vartheta = \frac{1}{a_1\rho}$.

Unfortunately, it is challenging to obtain a closed-form formula for the first integral in (34); as a result, we use the approximation technique.

It follows from the enlarged Taylor's series that $e^{-ax} = \sum_{k=0}^{K} (k!)^{-1}(-1)^k (ax)^k$ in which $K \in \{1, 2, \ldots, \infty\}$, then we get

$$\mathcal{E}_{D_1} = -\frac{1}{\zeta}\log_2\left[\frac{\left(\beta_{Q_n^1}\right)^{\alpha_{Q_n^1}} \vartheta^{\frac{\alpha_{Q_n^1}-2}{2}}}{2\Gamma\left(\alpha_{Q_n^1}\right)} \times \sum_{k=0}^{K} \frac{(-1)^k \left(\beta_{Q_n^1}\sqrt{\vartheta}\right)^k}{k!} \int_0^{\infty} \frac{x^{\frac{\alpha_{Q_n^1}+k-2}{2}}}{(1+x)^{\zeta}} dx\right]. \quad (35)$$

Finally, using [51, Eq. (3.194.3)], the expression of D_1's effective capacity may be given as

$$\mathcal{E}_{D_1} = -\frac{1}{\zeta}\log_2\left[\frac{\left(\beta_{Q_n^1}\right)^{\alpha_{Q_n^1}} \vartheta^{\frac{\alpha_{Q_n^1}-2}{2}}}{2\Gamma\left(\alpha_{Q_n^1}\right)} \sum_{k=0}^{K} \frac{(-1)^k \left(\beta_{Q_n^1}\sqrt{\vartheta}\right)^k}{k!\Gamma(\zeta)} \times \Gamma\left(\frac{\alpha_{Q_n^1}+k}{2}\right)\Gamma\left(\frac{2\zeta-\alpha_{Q_n^1}-k}{2}\right)\right]. \quad (36)$$

The proof is concluded.

APPENDIX D
PROOF OF PROPOSITION 4

Based on (19), we can formulate the expression of effective capacity at D_2 as

$$\mathcal{E}_{D_2} = -\frac{1}{\zeta}\log_2\left(\int_0^{\infty} (1+x)^{-\zeta} f_{\bar{\gamma}_{D_2}}(x)\, dx\right) = -\frac{1}{\zeta}\log_2\left[\frac{\left(\beta_{Q_n^2}\right)^{\alpha_{Q_n^2}}}{2\Gamma\left(\alpha_{Q_n^2}\right)} \int_0^{\frac{a_2}{a_1}} (1+x)^{-\zeta} \times \left(\frac{x}{\rho\left(a_2 - a_1 x\right)}\right)^{\frac{\alpha_{Q_n^2}-2}{2}} e^{-\beta_{Q_n^2}\sqrt{\frac{x}{\rho(a_2-a_1x)}}} dx\right]. \quad (37)$$

Let $t = \frac{2a_1}{a_2}x - 1 \to \frac{a_2(t+1)}{2a_1} = x \to \frac{a_2}{2a_1}dt = dx$, (37) can be calculated as

$$\mathcal{E}_{D_2} = -\frac{1}{\zeta}\log_2\left[\frac{a_2\left(\beta_{Q_n^2}\right)^{\alpha_{Q_n^2}}}{4a_1\Gamma\left(\alpha_{Q_n^2}\right)} \int_{-1}^{1} \left(1+\bar{\Lambda}(t)\right)^{-\zeta} \times \left(\frac{\bar{\Lambda}(t)}{\rho\left(a_2 - a_1\bar{\Lambda}(t)\right)}\right)^{\frac{\alpha_{Q_n^2}-2}{2}} e^{-\beta_{Q_n^2}\sqrt{\frac{\bar{\Lambda}(t)}{\rho\left(a_2-a_1\bar{\Lambda}(t)\right)}}} dt\right], \quad (38)$$

where $\bar{\Lambda}(t) = \frac{a_2(t+1)}{2a_1}$. Applying Chebyshev-Gauss quadrature [55], the effective capacity of D_2 can be calculated by

$$\mathcal{E}_{D_2} \approx -\frac{1}{\zeta}\log_2\left[\frac{\pi a_2\left(\beta_{Q_n^2}\right)^{\alpha_{Q_n^2}}}{4Pa_1\Gamma\left(\alpha_{Q_n^2}\right)} \sum_{p=1}^{P} \frac{\sqrt{1-\upsilon_p^2}}{\left(1+\bar{\Lambda}(\upsilon_p)\right)^{\zeta}} \times \left(\frac{\bar{\Lambda}(\upsilon_p)}{\rho\left(a_2 - a_1\bar{\Lambda}(\upsilon_p)\right)}\right)^{\frac{\alpha_{Q_n^2}-2}{2}} e^{-\beta_{Q_n^2}\sqrt{\frac{\bar{\Lambda}(\upsilon_p)}{\rho\left(a_2-a_1\bar{\Lambda}(\upsilon_p)\right)}}}\right], \quad (39)$$

where $\upsilon_p = \cos\left(\frac{2p-1}{2P}\pi\right)$. Thus, it is possible to get to (24). The proof is finished.

REFERENCES

[1] C. T. Nguyen, Y. M. Saputra, N. Van Huynh, T. N. Nguyen, D. T. Hoang, D. N Nguyen, V.-Q. Pham, M. Voznak, S. Chatzinotas, and D.-H. Tran, "Emerging technologies for 6G non-terrestrial-networks: From academia to industrial applications," 2024, *arXiv:2403.07763*.

[2] W. Saad, M. Bennis, and M. Chen, "A vision of 6G wireless systems: Applications, trends, technologies, and open research problems," *IEEE Netw.*, vol. 34, no. 3, pp. 134–142, May 2020.

[3] Y. Cui, F. Liu, X. Jing, and J. Mu, "Integrating sensing and communications for ubiquitous IoT: Applications, trends, and challenges," *IEEE Netw.*, vol. 35, no. 5, pp. 158–167, Sep. 2021.

[4] Z. Zhang and L. Dai, "Reconfigurable intelligent surfaces for 6G: Nine fundamental issues and one critical problem," *Tsinghua Sci. Technol.*, vol. 28, no. 5, pp. 929–939, Oct. 2023.

[5] M. Cui, Z. Wu, Y. Lu, X. Wei, and L. Dai, "Near-field MIMO communications for 6G: Fundamentals, challenges, potentials, and future directions," *IEEE Commun. Mag.*, vol. 61, no. 1, pp. 40–46, Jan. 2023.

[6] Y. Xu, G. Gui, H. Gacanin, and F. Adachi, "A survey on resource allocation for 5G heterogeneous networks: Current research, future trends, and challenges," *IEEE Commun. Surveys Tuts.*, vol. 23, no. 2, pp. 668–695, 2nd Quart., 2021.

[7] W. Yang, W. Xiang, Y. Yang, and P. Cheng, "Optimizing federated learning with deep reinforcement learning for digital twin empowered industrial IoT," *IEEE Trans. Ind. Informat.*, vol. 19, no. 2, pp. 1884–1893, Feb. 2023.

[8] W. Zhang, Y. Qin, W. Zhao, M. Jia, Q. Liu, R. He, and B. Ai, "A green paradigm for Internet of Things: Ambient backscatter communications," *China Commun.*, vol. 16, no. 7, pp. 109–119, Jul. 2019.

[9] R. Duan, X. Wang, H. Yigitler, M. U. Sheikh, R. Jantti, and Z. Han, "Ambient backscatter communications for future ultra-low-power machine type communications: Challenges, solutions, opportunities, and future research trends," *IEEE Commun. Mag.*, vol. 58, no. 2, pp. 42–47, Feb. 2020.

[10] Q. Wu and R. Zhang, "Towards smart and reconfigurable environment: Intelligent reflecting surface aided wireless network," *IEEE Commun. Mag.*, vol. 58, no. 1, pp. 106–112, Jan. 2020.

[11] C. Pan, H. Ren, K. Wang, J. F. Kolb, M. Elkashlan, M. Chen, M. Di Renzo, Y. Hao, J. Wang, A. L. Swindlehurst, X. You, and L. Hanzo, "Reconfigurable intelligent surfaces for 6G systems: Principles, applications, and research directions," *IEEE Commun. Mag.*, vol. 59, no. 6, pp. 14–20, Jun. 2021.

[12] A.-T. Le, T. N. Nguyen, L.-T. Tu, T.-P. Tran, T. T. Duy, M. Voznak, and Z. Ding, "Performance analysis of RIS-assisted ambient backscatter communication systems," *IEEE Wireless Commun. Lett.*, vol. 13, no. 3, pp. 791–795, Mar. 2024.

[13] C.-B. Le, D.-T. Do, X. Li, Y.-F. Huang, H.-C. Chen, and M. Voznak, "Enabling NOMA in backscatter reconfigurable intelligent surfaces-aided systems," *IEEE Access*, vol. 9, pp. 33782–33795, 2021.

[14] X. Gu, W. Duan, G. Zhang, Q. Sun, M. Wen, and P.-H. Ho, "Physical layer security for RIS-aided wireless communications with uncertain eavesdropper distributions," *IEEE Syst. J.*, vol. 17, no. 1, pp. 848–859, Mar. 2023.

[15] V.-D. Phan, B. C. Nguyen, T. M. Hoang, T. N. Nguyen, P. T. Tran, B. V. Minh, and M. Voznak, "Performance of cooperative communication system with multiple reconfigurable intelligent surfaces over Nakagami-*m* fading channels," *IEEE Access*, vol. 10, pp. 9806–9816, 2022.
[16] B. C. Nguyen, T. M. Hoang, P. T. Tran, T. N. Nguyen, V.-D. Phan, B. V. Minh, and M. Voznak, "Cooperative communications for improving the performance of bidirectional full-duplex system with multiple reconfigurable intelligent surfaces," *IEEE Access*, vol. 9, pp. 134733–134742, 2021.
[17] D. Tyrovolas, P.-V. Mekikis, S. A. Tegos, P. D. Diamantoulakis, C. K. Liaskos, and G. K. Karagiannidis, "Energy-aware design of UAV-mounted RIS networks for IoT data collection," *IEEE Trans. Commun.*, vol. 71, no. 2, pp. 1168–1178, Feb. 2023.
[18] T. Bai, C. Pan, Y. Deng, M. Elkashlan, A. Nallanathan, and L. Hanzo, "Latency minimization for intelligent reflecting surface aided mobile edge computing," *IEEE J. Sel. Areas Commun.*, vol. 38, no. 11, pp. 2666–2682, Nov. 2020.
[19] C. Huang, A. Zappone, G. C. Alexandropoulos, M. Debbah, and C. Yuen, "Reconfigurable intelligent surfaces for energy efficiency in wireless communication," *IEEE Trans. Wireless Commun.*, vol. 18, no. 8, pp. 4157–4170, Aug. 2019.
[20] Z. Gao, Y. Xu, Q. Wang, Q. Wu, and D. Li, "Outage-constrained energy efficiency maximization for RIS-assisted WPCNs," *IEEE Commun. Lett.*, vol. 25, no. 10, pp. 3370–3374, Oct. 2021.
[21] Q. Chen, M. Li, X. Yang, R. Alturki, M. D. Alshehri, and F. Khan, "Impact of residual hardware impairment on the IoT secrecy performance of RIS-assisted NOMA networks," *IEEE Access*, vol. 9, pp. 42583–42592, 2021.
[22] T. N. Nguyen, N. N. Thang, B. C. Nguyen, T. M. Hoang, and P. T. Tran, "Intelligent-reflecting-surface-aided bidirectional full-duplex communication system with imperfect self-interference cancellation and hardware impairments," *IEEE Syst. J.*, vol. 17, no. 1, pp. 1352–1362, Mar. 2023.
[23] N.-T. Nguyen, H.-N. Nguyen, N.-L. Nguyen, A.-T. Le, T. N. Nguyen, and M. Voznak, "Performance analysis of NOMA-based hybrid satellite-terrestrial relay system using mmWave technology," *IEEE Access*, vol. 11, pp. 10696–10707, 2023.
[24] D.-T. Vo, T. N. Nguyen, A.-T. Le, V.-D. Phan, and M. Voznak, "Holographic reconfigurable intelligent surface-aided downlink NOMA IoT networks in short-packet communication," *IEEE Access*, vol. 12, pp. 65266–65277, 2024.
[25] J. He, H. Wymeersch, and M. Juntti, "Channel estimation for RIS-aided mmWave MIMO systems via atomic norm minimization," *IEEE Trans. Wireless Commun.*, vol. 20, no. 9, pp. 5786–5797, Sep. 2021.
[26] A. Fascista, A. Coluccia, H. Wymeersch, and G. Seco-Granados, "RIS-aided joint localization and synchronization with a single-antenna mmWave receiver," in *Proc. IEEE Int. Conf. Acoust., Speech Signal Process. (ICASSP)*, Jun. 2021, pp. 4455–4459.
[27] Z. Ding and H. Vincent Poor, "A simple design of IRS-NOMA transmission," *IEEE Commun. Lett.*, vol. 24, no. 5, pp. 1119–1123, May 2020.
[28] X. Li, C. Zhang, C. He, G. Chen, and J. A. Chambers, "Sum-rate maximization in IRS-assisted wireless power communication networks," *IEEE Internet Things J.*, vol. 8, no. 19, pp. 14959–14970, Oct. 2021.
[29] C. H. Duc, S. Q. Nguyen, C.-B. Le, and N. T. V. Khanh, "Performance evaluation of UAV-based NOMA networks with hardware impairment," *Electronics*, vol. 11, no. 1, p. 94, Dec. 2021.
[30] T.-T. Nguyen, S. Q. Nguyen, P. X. Nguyen, and Y.-H. Kim, "Evaluation of full-duplex SWIPT cooperative NOMA-based IoT relay networks over Nakagami-*m* fading channels," *Sensors*, vol. 22, no. 5, p. 1974, Mar. 2022.
[31] T.-T. Nguyen and S. Q. Nguyen, "Short packet communications for cooperative UAV-NOMA-based IoT systems with SIC imperfections," *Comput. Commun.*, vol. 196, pp. 37–44, Dec. 2022.
[32] S. W. H. Shah, A. N. Mian, S. Mumtaz, A. Al-Dulaimi, I. Chih-Lin, and J. Crowcroft, "Statistical QoS analysis of reconfigurable intelligent surface-assisted D2D communication," *IEEE Trans. Veh. Technol.*, vol. 71, no. 7, pp. 7343–7358, Jul. 2022.
[33] V. Kumar, M. F. Flanagan, D. W. Kwan Ng, and L.-N. Tran, "On the secrecy rate under statistical QoS provisioning for RIS-assisted MISO wiretap channel," in *Proc. IEEE Global Commun. Conf. (GLOBECOM)*, Dec. 2021, pp. 1–6.
[34] D.-T. Do, T. T. Nguyen, C.-B. Le, M. Voznak, Z. Kaleem, and K. M. Rabie, "UAV relaying enabled NOMA network with hybrid duplexing and multiple antennas," *IEEE Access*, vol. 8, pp. 186993–187007, 2020.
[35] Z. Ding, Z. Yang, P. Fan, and H. V. Poor, "On the performance of non-orthogonal multiple access in 5G systems with randomly deployed users," *IEEE Signal Process. Lett.*, vol. 21, no. 12, pp. 1501–1505, Dec. 2014.
[36] Z. Ding, R. Schober, and H. V. Poor, "On the impact of phase shifting designs on IRS-NOMA," *IEEE Wireless Commun. Lett.*, vol. 9, no. 10, pp. 1596–1600, Oct. 2020.
[37] Z. Zhang, C. Zhang, C. Jiang, F. Jia, J. Ge, and F. Gong, "Improving physical layer security for reconfigurable intelligent surface aided NOMA 6G networks," *IEEE Trans. Veh. Technol.*, vol. 70, no. 5, pp. 4451–4463, May 2021.
[38] Z. Tang, T. Hou, Y. Liu, J. Zhang, and L. Hanzo, "Physical layer security of intelligent reflective surface aided NOMA networks," *IEEE Trans. Veh. Technol.*, vol. 71, no. 7, pp. 7821–7834, Jul. 2022.
[39] A.-T. Le, T. D. Hieu, T. N. Nguyen, T.-L. Le, S. Q. Nguyen, and M. Voznak, "Physical layer security analysis for RIS-aided NOMA systems with non-colluding eavesdroppers," *Comput. Commun.*, vol. 219, pp. 194–203, Apr. 2024.
[40] M. H. N. Shaikh, V. A. Bohara, A. Srivastava, and G. Ghatak, "A downlink RIS-aided NOMA system with hardware impairments: Performance characterization and analysis," *IEEE Open J. Signal Process.*, vol. 3, pp. 288–305, 2022.
[41] T. N. Nguyen, N. V. Vinh, B. C. Nguyen, and B. V. Minh, "On performance of RIS-aided bidirectional full-duplex systems with combining of imperfect conditions," *Wireless Netw.*, vol. 30, no. 2, pp. 649–660, Feb. 2024.
[42] M. You, H. Sun, J. Jiang, and J. Zhang, "Unified framework for the effective rate analysis of wireless communication systems over MISO fading channels," *IEEE Trans. Commun.*, vol. 65, no. 4, pp. 1775–1785, Apr. 2017.
[43] G. Li, H. Liu, G. Huang, X. Li, B. Raj, and F. Kara, "Effective capacity analysis of reconfigurable intelligent surfaces aided NOMA network," *EURASIP J. Wireless Commun. Netw.*, vol. 2021, no. 1, pp. 1–16, Dec. 2021.
[44] B. C. Nguyen, L. T. Dung, T. M. Hoang, N. V. Vinh, and G. T. Luu, "On performance of multi-RIS assisted multi-user nonorthogonal multiple access system over Nakagami-*m* fading channels," *Comput. Commun.*, vol. 197, pp. 294–305, Jan. 2023.
[45] C. Zhang, W. Yi, Y. Liu, Z. Ma, and X. Zhang, "NOMA for multi-cell RIS networks: A stochastic geometry model," *IEEE Trans. Wireless Commun.*, vol. 23, no. 8, pp. 10398–10413, Aug. 2024.
[46] D. Selimis, K. P. Peppas, G. C. Alexandropoulos, and F. I. Lazarakis, "On the performance analysis of RIS-empowered communications over Nakagami-*m* fading," *IEEE Commun. Lett.*, vol. 25, no. 7, pp. 2191–2195, Jul. 2021.
[47] T. L. Nguyen, T. N. Do, G. Kaddoum, D. B. D. Costa, and Z. J. Haas, "Channel characterization for RIS-aided terahertz communications: A stochastic approach," *IEEE Wireless Commun. Lett.*, vol. 11, no. 9, pp. 1890–1894, Sep. 2022.
[48] Q. Wu and R. Zhang, "Beamforming optimization for wireless network aided by intelligent reflecting surface with discrete phase shifts," *IEEE Trans. Commun.*, vol. 68, no. 3, pp. 1838–1851, Mar. 2020.
[49] P. M. Quang, N. T. Kien, T. T. Duy, N. H. An, N. T. Tung, and A. V. Le, "Performance evaluation of reconfigurable intelligent surface aided multi-hop relaying schemes with short packet communication," *Adv. Electr. Electron. Eng.*, vol. 22, no. 1, pp. 97–106, Mar. 2024.
[50] T. T. Dao, S. Q. Nguyen, H. Nhung-Nguyen, P. X. Nguyen, and Y.-H. Kim, "Performance evaluation of downlink multiple users NOMA-enable UAV-aided communication systems over Nakagami-*m* fading environments," *IEEE Access*, vol. 9, pp. 151641–151653, 2021.
[51] I. S. Gradshteyn and I. M. Ryzhik, *Table of Integrals, Series, and Products*. U.K.: Academic Press, 2014.
[52] D. Wu and R. Negi, "Effective capacity: A wireless link model for support of quality of service," *IEEE Trans. Wireless Commun.*, vol. 2, no. 4, pp. 630–643, May 2003.
[53] Y. Cheng, K. H. Li, Y. Liu, K. C. Teh, and H. Vincent Poor, "Downlink and uplink intelligent reflecting surface aided networks: NOMA and OMA," *IEEE Trans. Wireless Commun.*, vol. 20, no. 6, pp. 3988–4000, Jun. 2021.
[54] X. Li, H. Liu, G. Li, Y. Liu, M. Zeng, and Z. Ding, "Effective capacity analysis of AmBC-NOMA communication systems," *IEEE Trans. Veh. Technol.*, vol. 71, no. 10, pp. 11257–11261, Oct. 2022.
[55] M. Abramowitz and I. A. Stegun, *Handbook of Mathematical Functions With Formulas, Graphs, and Mathematical Tables*, vol. 55. New York, NY, USA: U.S. Government Printing Office, 1968.

TRAN CONG HUNG was born in Vietnam, in 1961. He received the B.E. degree (Hons.) in electronic and telecommunication engineering from Ho Chi Minh University of Technology, Vietnam, in 1987, the B.E. degree in informatics and computer engineering from Ho Chi Minh University of Technology, in 1995, the Master of Engineering degree in telecommunications engineering course from the Postgraduate Department, Hanoi University of Technology, Vietnam, in 1998, and the Ph.D. degree from Hanoi University of Technology, in 2004. Currently, he is an Associate Professor with the School of Computer Science and Engineering, The Saigon International University, Ho Chi Minh City, Vietnam. His main research interests include B-ISDN performance parameters and measuring methods, QoS in high-speed networks, and MPLS.

TAN N. NGUYEN (Member, IEEE) was born in Nha Trang, Vietnam, in 1986. He received the B.S. degree in electronics from Ho Chi Minh University of Natural Sciences, in 2008, the M.S. degree in telecommunications engineering from Vietnam National University, in 2012, and the Ph.D. degree in communications technologies from the Faculty of Electrical Engineering and Computer Science, VSB–Technical University of Ostrava, Czech Republic, in 2019. He joined the Faculty of Electrical and Electronics Engineering, Ton Duc Thang University, Vietnam, in 2013, and since then has been lecturing. His major research interests include cooperative communications, cognitive radio, signal processing, satellite communication, UAV, and physical layer security. He started as the Editor-in-Chief of *Advances in Electrical and Electronic Engineering* (AEEE) journal, in 2023.

VU QUANG SY was born in Thái Bình, Vietnam. He received the B.E., M.S., and Ph.D. degrees in electrical engineering from Peter the Great St. Petersburg State Polytechnic University, in 2012, 2014, and 2019, respectively. His research interests include electrical power engineering, power systems analysis, electromagnetic compatibility, and renewable energy technology.

ANH-TU LE (Member, IEEE) was born in Lam Dong, Vietnam, in 1997. He received the B.S. degree from the Industrial University of Ho Chi Minh City, Vietnam, in 2019, and the M.S. degree from Ton Duc Thang University, Vietnam, in 2022. He is currently pursuing the Ph.D. degree in communication technology with VSB–Technical University of Ostrava, Czech Republic. He has authored and co-authored more than 25 ISI-indexed journals. His research interests include wireless channel modeling, NOMA, cognitive radio, MIMO, and machine learning.

BUI VU MINH was born in Dong Nai, Vietnam, in March 1991. He received the degree in electrical and electronic engineering from Nguyen Tat Thanh University, Ho Chi Minh City, Vietnam, in 2015, and the master's degree in electrical engineering from Ho Chi Minh City University of Technology and Education, Ho Chi Minh City, in 2019. In 2014, he joined the Faculty of Engineering and Technology, Nguyen Tat Thanh University as Laboratory-Practice Management, until in 2017, he was a Lecturer. His major research interests include wireless networks, robot, artificial neural networks, and power electronics.

MIROSLAV VOZNAK (Senior Member, IEEE) received the Ph.D. degree in telecommunications from the Faculty of Electrical Engineering and Computer Science, VSB–Technical University of Ostrava, and the Habilitation degree, in 2009. He was appointed as a Full Professor of electronics and communications technologies, in 2017. He is currently a Principal Investigator in the research project QUANTUM5 funded by NATO, which focuses on the application of quantum cryptography in 5G campus networks. He participated in six projects funded by the EU in programs managed directly by European Commission. He has authored and co-authored more than 100 articles in SCI/SCIE journals. His research interests include ICT, especially on quality of service and experience, network security, wireless networks, and big data analytics. According to the Stanford University study released, in 2020, he is one of the World's Top 2% of Scientists in networking and telecommunications, and information and communications technologies. He has served as the General Chair for the 11th IFIP Wireless and Mobile Networking Conference, in 2018, and the 24th IEEE/ACM International Symposium on Distributed Simulation and Real-Time Applications, in 2020.